



UNIVERSITI  
MALAYSIA  
KELANTAN

**CHARACTERIZATION OF ALUMINA- GRAPHENE  
NANOCOMPOSITE PRODUCED BY  
HYDROTHERMAL METHOD FOR  
ENVIRONMENTAL APPLICATION**

by

**NUR FARIHAH BINTI MOHAMAD ISA**

A report submitted in fulfillment of the requirements for the degree of  
Bachelor of Applied Science (Materials Technology)

---

**FACULTY OF EARTH SCIENCE  
UNIVERSITI MALAYSIA KELANTAN**

---

2016

---

## ACKNOWLEDGEMENTS

I wish to thank various people for their contribution in this project. Without them this research will not be completed successfully.

I would like to express my great appreciation to my research supervisor, Dr. Mahani binti Yusoff for her patient guidance, enthusiastic encouragement and useful critiques of this research work. Thanks also to Dr. Nik Raihan binti Nik Yusof for her guidance and assistance in finishing this research. My grateful thanks also extended to Dr. Mohamad Najmi bin Masri and Dr. Mohd Hazim bin Mohamad Amini for their constructive critiques and recommendations in this research.

Moreover, I would to extend my thanks to the technicians and lab assistants of Faculty Earth Science for their valuable technical supports and helped me in handling instruments. I also wish to thanks all my friends in helping and encourage me in this research work.

Last but not least, a deep gratitude for my parents and family for their support and encouragement throughout my study.

UNIVERSITI  
MALAYSIA  
KELANTAN

## TABLE OF CONTENTS

	PAGE
<b>TITLE PAGE</b>	<b>i</b>
<b>AKNOWLEDGEMENTS</b>	<b>ii</b>
<b>TABLE OF CONTENTS</b>	<b>iii</b>
<b>LIST OF TABLES</b>	<b>vi</b>
<b>LIST OF FIGURES</b>	<b>vii</b>
<b>LIST OF ABBREVIATIONS</b>	<b>viii</b>
<b>ABSTRACT</b>	<b>ix</b>
<b>ABSTRAK</b>	<b>x</b>
<b>CHAPTER 1 INTRODUCTION</b>	
1.1 Background of study	1
1.2 Problem Statement	3
1.3 Objectives	4
1.4 Expected Outcomes	4
<b>CHAPTER 2 LITERATURE REVIEWS</b>	
2.1 Nanocomposites	5
2.1.1 Metal Matrix Nanocomposites	6
2.1.2 Polymer Matrix Nanocomposites	6
2.1.3 Ceramic Matrix Nanocomposites	6
2.2 Nanocomposite matrices	7
2.2.1 Titanium oxide	7
2.2.2 Silica	8

2.2.3	Zirconia	8
2.2.4	Alumina	9
2.3	Reinforcement in ceramic matrix	11
2.3.1	Silicon Nitride	11
2.3.2	Carbon Nanotubes	12
2.3.3	Silver nanoparticles	13
2.3.4	Graphene	14
2.4	Fabrication methods	15
2.4.1	Powder Processing	16
2.4.2	Colloidal Processing	17
2.4.3	Sol-Gel Method	18
2.4.4	Hydrothermal method	18
2.5	Nanocomposite for wastewater application	19
2.6	Degradation of dyes in water	19
2.7	Photocatalytic degradation using nanocomposite	20
<b>CHAPTER 3 MATERIALS AND METHODS</b>		
3.1	Introduction	23
3.2	Materials	23
3.3	Preparation of Al <sub>2</sub> O <sub>3</sub> -graphene nanocomposite	23
3.4	Characterization of Al <sub>3</sub> O <sub>2</sub> -graphene nanocomposite	25
3.4.1	Phase Identification	25
3.4.2	Crystallite Size and Internal Strain	26
3.4.3	Morphology	26

3.4.4	Functional Group	26
3.4.5	Photocatalytic Performance	26
<b>CHAPTER 4 RESULTS AND DISCUSSION</b>		
4.1	Phase Identification	28
4.2	Crystallite Size and Internal Strain	30
4.3	Morphology	31
4.4	Functional group	32
4.5	Absorption of MO dye	34
<b>CHAPTER 5 CONCLUSION AND RECOMMENDATION</b>		
5.1	Conclusion	36
5.2	Recommendation	37
<b>REFERENCES</b>		38
Appendix A		41
Appendix B		42

## LIST OF TABLES

Table 2.1	Different types of nanocomposite (Camargo <i>et al.</i> , 2009)	5
Table 3.1	Composition of Al <sub>2</sub> O <sub>3</sub> and graphene to produce nanocomposite	25
Table 4.1	The crystallite size and internal strain of Al <sub>2</sub> O <sub>3</sub> -graphene nanocomposite	31



## LIST OF FIGURES

Figure 2.1	SEM micrographs of $Al_2O_3$ powder (Tabandeh-Khorshid <i>et al.</i> , 2016)	10
Figure 2.2	Carbon nanotubes (CNTs) (Baksi & Biswas, 2014)	12
Figure 2.3	After CNT/ZnO nanorods synthesis (Bai <i>et al.</i> , 2015)	13
Figure 2.4	SEM image of 3% TG (Zargari <i>et al.</i> , 2016)	15
Figure 2.5	Overview for graphene synthesis methods (Porwal <i>et al.</i> , 2013)	16
Figure 2.6	Conventional powders processing of $Al_2O_3$ -SiC nanocomposite (Camargo <i>et al.</i> , 2009)	17
Figure 2.7	Visible light-energized photocatalytic degradation of MO (Hua <i>et al.</i> , 2015)	21
Figure 2.8	Energy band diagram (Hua <i>et al.</i> , 2015)	22
Figure 3.1	Flow chart of the research	24
Figure 4.1	XRD patterns of pure a) graphene and b) $Al_2O_3$ with compositions c)AG50, d)AG60, e)AG70, f)AG80 and g)A100	29
Figure 4.2	Plot of $Br \cos \theta$ against $\sin \theta$ in a)AG50, b)AG60, c)AG70, d)AG80, and e)A100	30
Figure 4.3	The optical images of pure a) $Al_2O_3$ and b)graphene before hydrothermal process	31
Figure 4.4	The optical images of a)A100, b)G100, c)AG50, d)AG60, e)AG70 and f)AG80 after hydrothermal process	32
Figure 4.5	FTIR spectra of $Al_2O_3$ graphene nanocomposite of pure a) $Al_2O_3$ and b)graphene with compositions c)AG50, d)AG60, e)AG70, f)AG80 and g)A100.	33
Figure 4.6	The percentage of MO absorption for a)1, b)2, c)3 and d)4 hours.	34

## LIST OF ABBREVIATIONS

<b>Abbreviation</b>	<b>Description</b>
AR	Anti-reflection
CNT	Carbon nanotube
CMNC	Ceramic matrix nanocomposite
DA	Dopamine
FTIR	Fourier Transformation Infrared Spectrophotometer
MB	Methylene blue
MO	Methyl orange
MF	Microfiltration
MMNC	Metal matrix nanocomposite
MWCO	Molecular weight of the solute
PMNC	Polymer matrix nanocomposite
PECVD	Plasma-enhanced chemical vapour deposition
RhB	Rhodamine blue
SEM	Scanning Electron Microscope
TFN	Thin film nanocomposite
TMOS	Tetramethyl orthosilicate
UF	Ultrafiltration
XRD	X-ray Diffraction
UV	Ultra violet
UV-vis	Ultraviolet-visible spectroscopy



# **CHARACTERIZATION OF ALUMINA- GRAPHENE NANOCOMPOSITE PRODUCED BY HYDROTHERMAL METHOD FOR ENVIRONMENTAL APPLICATION**

## **ABSTRACT**

In this study, the performance of Al<sub>2</sub>O<sub>3</sub>-graphene nanocomposite towards methyl orange (MO) dye were examined. The aims of this study were to characterize the Al<sub>2</sub>O<sub>3</sub>-graphene nanocomposite produced by hydrothermal method and to study the performance of Al<sub>2</sub>O<sub>3</sub>-graphene nanocomposite towards absorption of MO. Al<sub>2</sub>O<sub>3</sub>-graphene nanocomposite was prepared by hydrothermal method at 200°C. The result showed the crystallite size of Al<sub>2</sub>O<sub>3</sub> is decreased and internal strain increased with the increase of graphene content. The particle size of nanocomposite becomes larger with the increment graphene amount in the nanocomposite. Nanocomposite with lower graphene (20wt%) contents and higher Al<sub>2</sub>O<sub>3</sub> (80wt%) contents performed the best for the MO absorption with efficiency of 75% in visible light.

UNIVERSITI  
MALAYSIA  
KELANTAN

## **PRESTASI ALUMINA- GRAFEN NANOKOMPOSIT YANG DIHASILKAN DARIPADA KAEDAH HIDROTERMAL UNTUK APLIKASI PERSEKITARAN**


### **ABSTRAK**

Prestasi  $\text{Al}_2\text{O}_3$ -grafen nanokomposit terhadap pewarna metil jingga telah dilaksanakan. Tujuan kajian ini dilakukan adalah untuk mencirikan  $\text{Al}_2\text{O}_3$ -grafen nanokomposit yang dihasilkan daripada kaedah hidrotermal dan untuk mengkaji prestasi  $\text{Al}_2\text{O}_3$ -grafen nanokomposit terhadap penyerapan metil jingga.  $\text{Al}_2\text{O}_3$ -grafen nanokomposit telah berjaya disintesis daripada kaedah hidrotermal pada suhu  $200^\circ\text{C}$ . Keputusan menunjukkan saiz kumin hablur  $\text{Al}_2\text{O}_3$  semakin mengecil dan terikan dalaman meningkat apabila kandungan grafen semakin meningkat. Saiz zarah nanokomposit ini juga semakin bertambah akibat daripada kenaikan jumlah grafen di dalam nanokomposit. Nanokomposit dengan kandungan grafen yang rendah (20% wt) dan kandungan  $\text{Al}_2\text{O}_3$  yang tinggi (80% wt) berprestasi yang terbaik untuk penyerapan metil jingga dengan kadar kecekapan sebanyak 75% di bawah cahaya tampak.

UNIVERSITI  
MALAYSIA  
KELANTAN

## DECLARATION

I hereby declare that the work embodied in this report is the result of the original research and has not been submitted for a higher degree to any universities or institutions.

  
\_\_\_\_\_

Student

Name: NUR FARIYAH BINTI MOHAMAD ISA

Date: 1/1/17

I certify that the Report of this final year project entitled "Characterization of Alumina-graphene Nanocomposite Produced by Hydrothermal Method for Environmental Application" by Nur Fariyah binti Mohamad Isa, matric number E13A199 has been examined and all the correction recommended by examiners have been done for the degree of Bachelor of Applied Science (Materials Technology) with Honours, Faculty of Earth Science, Universiti Malaysia Kelantan.

Approved by:



Supervisor: DR. MAHANI BINTI YUSOFF

Name: Pensyarah Kanan  
Teknologi Bahan  
Fakulti Sains Bumi  
Universiti Malaysia Kelantan

Date: 1/1/2017

# CHAPTER 1

## INTRODUCTION

### 1.1 Background of study

Nanocomposite is an improvement from microcomposite which alter the limitations in the microcomposite and monolithic. It appears that the smaller the particle size exhibit better in physical and chemical properties of that material. The advantages of nanocomposite are the enhanced properties of the products, lessen the solid wastes with the lower gauge thickness films and lower reinforcement usage and improvement in manufacturing capability for packaging applications.

Nanoparticles can be used either for the matrix or the reinforcement to produce nanocomposite. The major function of matrix in the composite is to bind the fibers together, provides rigidity and shape to the structure and gives corrosion and wear protection for fibers. Each type of matrix material is possible in different applications based on their abilities in the nanocomposites (Camargo *et al.*, 2009). There are three types of nanocomposite which are metal-matrix nanocomposite (MMNC), polymer-matrix nanocomposite (PMNC) and ceramic-matrix nanocomposite (CMNC). Among them, CMNC is the most used for high temperature application and wear resistance. Moreover, CMNC also offers high hardness and strength. Examples of ceramic matrices that have been commonly used in the application of high temperature are titania ( $\text{TiO}_2$ ), silica ( $\text{SiO}_2$ ), zirconia ( $\text{ZrO}_2$ ) and alumina ( $\text{Al}_2\text{O}_3$ ).

$\text{Al}_2\text{O}_3$  is the most widely used ceramic matrix to produce composite due to low price, high hardness and chemical stability (Yazdani *et al.*, 2015).  $\text{Al}_2\text{O}_3$  also possess high thermal conductivity, melting point and thermal expansion making it

possible for high temperature application (Trunec *et al.*, 2015). However,  $\text{Al}_2\text{O}_3$  suffers from low fracture toughness (Dong *et al.*, 2009; Hanzel *et al.*, 2015). Therefore,  $\text{Al}_2\text{O}_3$  is reinforced with nanoparticles such as carbon nanotube (Porwal *et al.*, 2015), titanium nanoparticles (Yoon *et al.*, 2015) and silver nanoparticles (Chaker *et al.*, 2016). Moreover,  $\text{Al}_2\text{O}_3$  has potential to be functionalized in environmental application as  $\text{Al}_2\text{O}_3$  has properties that could reduce the band gap of the materials (Barajas-Ledesma *et al.*, 2010). However,  $\text{Al}_2\text{O}_3$  is seldom reinforced with graphene and to be used for environmental application for degradation of dyes.

Reinforcement of the composite is defined as binder that combines the two materials together. Reinforcement usually carries the load of the composite for about 70 to 90% by fibers. The reinforced materials provide structural properties such as stiffness, strength and thermal stability to the composite. The examples of the reinforcement materials used as reinforced phase in  $\text{Al}_2\text{O}_3$  are silicon nitride ( $\text{Si}_3\text{N}_4$ ) (Ramdani *et al.*, 2014), carbon nanotube (CNT) (Long *et al.*, 2015) and silver nanoparticles (Chaker *et al.*, 2016).

$\text{Al}_2\text{O}_3$ -based nanocomposite has been found mostly on high temperature application. However, there is limited information regarding the performance of  $\text{Al}_2\text{O}_3$ -based nanocomposite in waste water application. Recently, graphene gains the interest of the most researchers to become reinforcement in the nanocomposite (Liu *et al.*, 2015). Graphene with structure of two-dimensional (2D) honeycomb lattice is also an ideal candidate to be reinforced with  $\text{Al}_2\text{O}_3$ . This is because graphene exhibits excellent electrical and mechanical properties (Liu *et al.*, 2015). Graphene displays a good compatibility with  $\text{Al}_2\text{O}_3$  nanocomposite that can enhanced the mechanical properties of nanocomposite (Spanos *et al.*, 2015; Simoes *et al.*, 2015; Drakonakis *et al.*, 2014) so that it can be used for waste water application.

Therefore, this study used Al<sub>2</sub>O<sub>3</sub>-graphene nanocomposite to degrade the dyes in wastewater treatment.

There are many methods that can be used to disperse graphene in the ceramic-based nanocomposite. Such examples are colloidal processing, powder processing, sol-gel method and hydrothermal method. In this study, hydrothermal method is used as fabrication method of Al<sub>2</sub>O<sub>3</sub>-graphene nanocomposite. Hydrothermal is a low cost synthesise method uses to produce metal or metal oxide form aqueous solution by applying temperature and pressure in an autoclave. This method can be used to synthesise ceramic-based nanocomposite for waste water application.

The aim of the research is to evaluate the characteristics of Al<sub>2</sub>O<sub>3</sub>-graphene nanocomposite produced by hydrothermal method. The performance of Al<sub>2</sub>O<sub>3</sub>-graphene nanocomposite also will be studied towards the degradation of dyes to be applied in environmental application.

## **1.2 Problem statement**

Al<sub>2</sub>O<sub>3</sub>-graphene nanocomposite is commonly utilized in biomedical application. Nevertheless, there are a little research has been conducted so far to make Al<sub>2</sub>O<sub>3</sub>-graphene nanocomposite using hydrothermal method for the use in environmental application. Hence, in this study, hydrothermal method is used in synthesising graphene in Al<sub>2</sub>O<sub>3</sub> matrix to produce nanocomposite.

Al<sub>2</sub>O<sub>3</sub>-graphene nanocomposite has been synthesized using colloidal and powder processing. Colloidal processing is a technique to produce enhanced of degree of dispersion with modification of surface charges on ceramic and graphene powder. On the other hand, powder processing is a technique where the filler

material need to de-agglomerated using numerous methods including ultrasonication and mixed with ceramic powder in a solvent to produce slurries of dispersed ceramics. Both methods commonly used in reinforcing graphene in ceramic matrix. However, these methods are uneconomical and not environmental friendly.

This study also involves evaluation of absorption the methyl orange using photocatalytic properties of  $\text{Al}_2\text{O}_3$ -graphene nanocomposite for environmental application which is mostly used in wastewater treatment in textile industry.

### **1.3 Objectives**

The objectives of this research are:

- 1) To evaluate the characterization of  $\text{Al}_2\text{O}_3$ -graphene nanocomposite produced by hydrothermal method.
- 2) To study the performance of  $\text{Al}_2\text{O}_3$ -graphene nanocomposite towards absorption of methyl orange.

### **1.4 Expected outcomes**

The different composition of graphene will influence the structural properties and dispersion of graphene within the  $\text{Al}_2\text{O}_3$  matrix. The hydrothermal synthesis at  $200^\circ\text{C}$  will also affect the photocatalytic degradation of MO in wastewater application.

## CHAPTER 2

### LITERATURE REVIEW

#### 2.1 Nanocomposite

Nanocomposite is composite that has dimension within nanometer range ( $1\text{nm} = 10^{-9}\text{ m}$ ). It has been reported that particles in nanometer range can perform better in term of their properties than in micrometer size such as catalytic activity, hardness and plasticity and refractive index (Camargo *et al.*, 2009). Nanocomposite is classified into three types which are ceramic matrix nanocomposites (CMNC), metal matrix nanocomposites (MMNC) and polymer matrix nanocomposites (PMNC) as stated by Camargo *et al.*, (2009). Table 2.1 shows different types of nanocomposite that has been synthesised of the most researchers.

Table 2.1 Different types of nanocomposite (Camargo *et al.*, 2009)

Class	Examples
Metal	FeCr/Al <sub>2</sub> O <sub>3</sub> , Ni/Al <sub>2</sub> O <sub>3</sub> , Co/Cr, Fe/MgO, Al/CNT, Mg/CNT
Polymer	Thermoplastic/thermoset polymer/layered silicates, polyester/TiO <sub>2</sub> , polymer/CNT, polymer/layered double hydroxides.
Ceramic	Al <sub>2</sub> O <sub>3</sub> /SiO <sub>2</sub> , SiO <sub>2</sub> /Ni, Al <sub>2</sub> O <sub>3</sub> /TiO <sub>2</sub> , Al <sub>2</sub> O <sub>3</sub> /SiC, Al <sub>2</sub> O <sub>3</sub> /CNT

Nanocomposite can be used in various applications such as sensors, supercapacitors and industry purposes. Nurzulaikha *et al.*, (2015) proposed graphene-tin oxide nanocomposite used in medical application to detect dophamine (DA), an organic chemical that is hazardous if it is in abnormal level in the human body. Moreover, molybdenum sulphide and N-doped graphene hybrid



nanocomposites can enhanced the superconductor performance by increasing the electrochemical properties of the nanocomposites (Xie *et al.*, 2016).

### **2.1.1 Metal-matrix nanocomposite**

MMNC is the material which consists of a ductile metal or alloy matrix that implanted in some nanosized materials. This type of nanocomposite can be classified as continuous and non-continuous reinforced materials (Pandiyarajan *et al.*, 2015). Camargo *et al.*, (2009) stated that this composite is suitable for high temperature and high shear or strength applications. This is due to the combination of metal and ceramic in the composite itself making it better in ductility and enhanced toughness.

### **2.1.2 Polymer-matrix nanocomposites**

Camargo *et al.*, (2009) stated that PMNC is produced by adding nanoparticulates to a polymer matrix which can strengthen the properties and performance of the nanocomposite. These types of nanocomposites are mostly used in the industry because they are lightweight and ductile. However, this nanocomposite is often added with fibers, platelets, particles and whiskers to improve the low modulus and strength properties of this nanocomposite. Such examples of polymer-matrix nanocomposites that proved to enhance in tensile strength and modulus are polypropylene/montmorillonite, polyester/TiO<sub>2</sub> and epoxy/layered-silicates.

### **2.1.3 Ceramic-matrix nanocomposites**

This group of nanocomposites are occupied by large volume of ceramic from the group of oxides, nitrides, borides, silicates and others (Pandiyarajan & Muthusankar, 2015). Ceramic-based nanocomposite becomes increasingly popular

because of their ability to work at high-temperature conditions as well as a promising photocatalytic material. Potential ceramics materials to be matrix in nanocomposite include titania ( $\text{TiO}_2$ ), silica ( $\text{SiO}_2$ ) and alumina ( $\text{Al}_2\text{O}_3$ ). The combination of these materials making nanocomposite possess significant enhancement in fracture strength and toughness, high temperature strength and creep resistance compared with its counterpart (Pandiyarajan *et al.*, 2015).

CMNC or ceramic-based nanocomposite has potential in decomposing organic pollutants in waste water. Several studies have proved that graphene is an ideal carbon material that used to involve in the product of semiconductor to improve the photocatalytic efficiency of the semiconductor to be used in wastewater application. Chen *et al.*, (2013) confirmed that  $\text{Ag}_3\text{PO}_4$ /graphene-oxide composite showed an enhancement in photocatalytic activity of dyes in water. Moreover, a research by Hua *et al.*, (2015) stated that nitrogen-doped perovskite-type  $\text{La}_2\text{TiO}_7$  on the graphene composite enhanced the photocatalytic activity toward bisphenol A in water.

## **2.2 Nanocomposites matrices**

The examples of matrix in the nanocomposite are  $\text{TiO}_2$ ,  $\text{SiO}_2$  and  $\text{ZrO}_2$ . These materials are often used in the research as they have good properties in terms of physical, chemical and thermal behaviours.

### **2.2.1 Titanium Oxide**

$\text{TiO}_2$  is mostly used in semiconductor fabrication material for photochemical purposes. The properties of this material are stable, biologically and chemically inert, non-toxic and not expensive (Chaker *et al.*, 2016).  $\text{TiO}_2$  also been used as a protective layer to prevent steel corrosion as reported by Leonard *et al.*, (2016).

This is due to the material exhibits anti-corrosive protection, photocatalytic activity and super hydrophilicity making it accessible with low fouling and reduced corrosion. However, Chaker *et al.*, (2016) showed that TiO<sub>2</sub> suffers from narrow light response range. This is because TiO<sub>2</sub> has a wide band gap and low separation efficiency of electron-hole pairs ( Li *et al.*, 2011; Chen *et al.*, 2016).

### 2.2.2 Silica

SiO<sub>2</sub> is one of the most widely used as reinforcement due to its high chemical stability, good mechanical strength, has porous structure and wide surface area. SiO<sub>2</sub> (n=1.4-1.5) is a transparent and high reflective index material. It is chosen as antireflection (AR) coating that is used in silicon (Si) solar cells to increase the photocurrent and photovoltaic efficiency (Jannat *et al.*, 2016).

In the research made by Cao *et al.*, (2016), the successful dispersion of SiO<sub>2</sub> in the raspberry-like gold (Au) made the nanocomposite possess high catalytic activity towards the reduction of p-nitrophenol (p-NPh) and also has good recyclability. This is proved by the increasing of catalytic activity of the Au/SiO<sub>2</sub> nanocomposite with the increased of HAuCl<sub>4</sub> loading and the reaction temperature which are 0.043-0.170g and 25-40°C respectively.

### 2.2.3 Zirconia

This ceramic material is widely used to be reinforced with other ceramic materials in order to strengthen the properties of ZrO<sub>2</sub>. Example of reinforced material that is commonly used is Al<sub>2</sub>O<sub>3</sub>. This Al<sub>2</sub>O<sub>3</sub>-ZrO<sub>2</sub> nanocomposite is widely used in the research due to the high mechanical properties and chemical inertness (Benavente *et al.*, 2014). However, majority of the studies were more focus on the fabrication method since it is important to decrease the grain size so that the

mechanical properties of the nanocomposite could be enhanced (Chinelatto *et al.*, 2014).

A research by Nemade *et al.*, (2014) synthesized the  $\text{Al}_2\text{O}_3\text{-ZrO}_2$  nanocomposite using spray pyrolysis technique to test the photocatalytic degradation of methylene blue (MB). From his research, the photodegradation capability of  $\text{Al}_2\text{O}_3\text{-ZrO}_2$  nanocomposite was around 3% after 36 minutes. However, the nanocomposite possesses high recycling capability and stability due to the rough surface nature of the nanocomposite when observed with Scanning Electron Microscope (SEM).

#### **2.2.4 Alumina**

Based on the review made by Davis (2010),  $\text{Al}_2\text{O}_3$  is a metal oxide that exists in nature as the minerals corundum ( $\text{Al}_2\text{O}_3$ ); diaspore ( $\text{Al}_2\text{O}_3\cdot\text{H}_2\text{O}$ ); gibbsite ( $\text{Al}_2\text{O}_3\cdot 2\text{H}_2\text{O}$ ); most commonly as bauxite, that is impure form of gibbsite. Figure 2.1 shows the micrograph of  $\text{Al}_2\text{O}_3$  powder from SEM.  $\text{Al}_2\text{O}_3$  is often used as a starting material for the smelting of aluminium metal, as a raw material for advanced ceramic product and as an active agent in chemical processing. Its application in ceramic industry such as insulating material, electronics, military uses, biomedical and many others because of its abundance and has multiple forms as well as its properties of stability, purity and refractoriness. However, due to the birefringent behaviour and difficulties of manufacturing nanocrystalline alumina ceramics, the transparency in the visible wavelength region is narrow and hence the applications of  $\text{Al}_2\text{O}_3$  in visible light are exceptional so far (Trunec *et al.*, 2015).

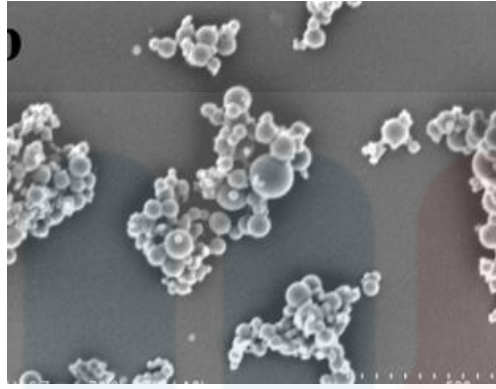


**Figure 2.1:** SEM micrographs of Al<sub>2</sub>O<sub>3</sub> powder (Tabandeh-Khorshid *et al.*, 2016)

Moreover, recent research shows Al<sub>2</sub>O<sub>3</sub> has been an interesting material due to their incredible properties in terms of physical, mechanical and thermal for various applications (Centano *et al.*, 2013; Yazdani *et al.*, 2014; Hanzel *et al.*, 2014). This ceramic material possesses low friction, high strength, high wear resistance and good corrosion resistance making it is widely used in biomedical application (Gutierrez-Gonzalez *et al.*, 2015).

According to Centeno *et al.*, (2013), Al<sub>2</sub>O<sub>3</sub> is a very interesting ceramic material to be used in technological applications. However, this material is lack of fracture toughness because of the limited in dislocation movement by their ionic or covalent bonds as stated by Hanzel *et al.*, (2014). In order to overcome this problem, an addition of particulates such as ceramic and metal could alter the brittleness of Al<sub>2</sub>O<sub>3</sub> (Yazdani *et al.*, 2014) .

Researchers showed that Al<sub>2</sub>O<sub>3</sub>-based nanocomposite has potential in technological and environmental applications. Pei *et al.*, (2014) studied the catalytic effect of Fe<sup>3+</sup> modified nanometer TiO<sub>2</sub> loaded on Al<sub>2</sub>O<sub>3</sub>. The results proved that the best photocatalytic effect was achieved with 10% of TiO<sub>2</sub> composite making the degradation rates are 0.71%, 3.9%, 1.3% and 15.1% larger than unloaded TiO<sub>2</sub>.

This showed that the prepared nanocomposite has potential to be used as semiconductor optical catalyst for reduction of harmful gas in automobile exhaust due to the good degradation of organic pollutants.

However, there is a little research has been made to produce  $\text{Al}_2\text{O}_3$ -graphene nanocomposite to analyse its potential in the environmental application by exploring its photocatalytic degradation towards dyes.

### **2.3 Reinforcements in ceramic matrix**

Reinforced materials need to be analysed their properties as their main function is to enhance the matrix in the nanocomposite. The selection of suitable materials is important because this will determine their properties in the dispersion of matrix in the nanocomposite. The most used reinforced materials in  $\text{Al}_2\text{O}_3$ -based nanocomposite the recent research are silicon nitrides ( $\text{Si}_3\text{N}_4$ ) (Ramdani *et al.*, 2014), carbon nanotubes (CNT) (Simões *et al.*, 2015) and graphene (Liu *et al.*, 2015) are used in various application.

#### **2.3.1 Silicon Nitrides**

$\text{Si}_3\text{N}_4$  is a ceramic fillers that are investigated for its high strength and high toughness which can replace metals for much high temperature applications. This material exhibits high resistance to corrosion, wear properties with low dielectric constant, low density and high hardness (Ramdani *et al.*, 2014).

In the research carried out by Ramdani *et al.*, (2014), polybenzoxazine nanocomposite reinforced with  $\text{Si}_3\text{N}_4$  nanoparticles could improves the tensile strength which increased to 30wt%. Moreover, the thermal and mechanical

properties also enhanced with better adhesion of  $\text{Si}_3\text{N}_4$  inside the polybenzoxazine matrix.

### 2.3.2 Carbon Nanotubes

CNT is carbon-based fillers which are commonly used in nanocomposite research to improve structural and functional properties of host materials. Figure 2.2 shows the structure of CNT material. This material possesses the stiffest and strongest materials ever found as stated by Long *et al.*, (2015). Two categories of CNT are discovered which are single wall CNT and multiple wall CNT.

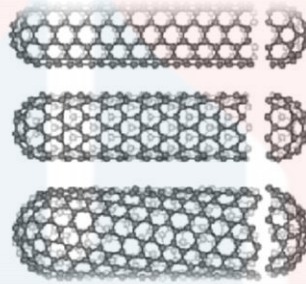


**Figure 2.2:** Carbon Nanotubes (CNTs) (Baksi & Biswas, 2014)

Experimental research by Long *et al.*, (2015) proved that small amount of CNT dispersed in the copper matrix increased the nanocomposite strength about 300% by a novel electrochemical co-deposition. Moreover, the past research proved that carbon nanotubes (CNT) as a filler in  $\text{Al}_2\text{O}_3$  matrix led to the enhancement of mechanical properties (Thomson *et al.*, 2012; Estili & Sakka, 2014; Sarkar & Das, 2014). In the research carried out by Simoes *et al.*, (2015), aluminium matrix nanocomposites reinforced by CNT revealed an enhanced of 50% in the hardness and 200% in the tensile strength as compared with pure aluminium produced via classical powder metallurgy route. However, CNT has other disadvantages as it is hard to process, expensive and more health hazards as compared to graphene.

In photodegradation of dyes, CNT commonly used as a reinforcement material as done by Bai *et al.*, 2015. In this research, CNT is doped with ZnO and TiO<sub>2</sub> as a nanocomposite ultrafiltration (UF) membrane synthesised by hydrothermal method. Fig 2.3 showed the SEM micrograph image of synthesis of CNT/ZnO nanorods. After a series of photocatalytic oxidation test as well as membrane flux along with molecular weight of the solute (MWCO) rejection test, the research proved that this nanocomposite membrane showed a loose UF yet tight MF membrane that possessed photodegradation capacity, high membrane flux and low fouling potential.



**Figure 2.3:** After CNT/ZnO nanorods synthesis (Bai *et al.*, 2015)

### 2.3.3 Silver nanoparticles

Silver (Ag) has been utilized for centuries as microbial agents. This material in nano-size has high antimicrobial activity due to the large specific-surface compared to the bulk silver metal (Sadeghi *et al.*, 2012; Taheri *et al.*, 2014; Sedki *et al.*, 2015). In the wastewater application, a research made by Duran-Alvarez *et al.*, (2015) was doping mono-Ag and bi-metallic Au-Ag nanoparticles with TiO<sub>2</sub> to photocatalytically degrade the antibiotic ciprofloxacin in pure water using UV-C or simulated sunlight.



Ag also acts as noble metal which can be used as electron sinks, reduces the photo-generated e-/h+ recombination and also facilitates the charge separation. Moreover, Ag in the state of ions is interesting as its noble effects on the improvement of photoactivity and its bacterial properties (Kuriakose *et al.*, 2014; Deng *et al.*, 2012; Duan *et al.*, 2006). In the research made by Munoz-Fernandez *et al.*, (2016), it was found that the presence of Ag greatly enhanced the photocatalytic activity of the Ag/ZnO nanocomposite. The presence of Ag also effect in the well-dispersed nanoparticles in the nanocomposite compared to the pure ZnO sample.

#### **2.3.4 Graphene**

Graphene is an ideal reinforcement material in nanocomposite due to its superior properties in electrical, mechanical and thermal properties (Chen *et al.*, 2016; Rutkowski *et al.*, 2015). Kim *et al.*, (2014) stated that graphene protects the surface from wear environment and prevent falling out of Al<sub>2</sub>O<sub>3</sub> grains when embedded inside the Al<sub>2</sub>O<sub>3</sub> matrix. This will eventually enhance the mechanical property of Al<sub>2</sub>O<sub>3</sub>-graphene nanocomposite.

However, graphene content in the nanocomposite has a limitation. The higher the graphene content will result in decrease of the mechanical properties of the nanocomposites. Chen *et al.*, (2016) proved that when the graphene content in the copper matrix increases to 4.0 vol.%, the tensile dropped to 200 MPa after achieves 310 MPa at the graphene content of 0.6 vol.%. Moreover, when the elastic modulus and hardness of Cu/GNPs is graphed, it decreased after achieved certain unit of graphene content. Hence, the graphene content is an important controlled parameter so that the mechanical properties of the nanocomposite could be improved.

In the photocatalytic degradation for wastewater application, the research made by Zargari *et al.*, (2016) used nanostructured material of pillared graphene made of tin porphyrin functionalized graphene-TiO<sub>2</sub> composite (TG) to study the effect of graphene as dye sensitization on the photoactivity of the catalysts. The photocatalytic properties and photocurrent responses of the nanocomposite was examined and the result shows a high activity in the photodegradation reaction under irradiation of visible light. The result shows the nanocomposite containing 3% of graphene (3%TG) possesses the highest photoactivity. Figure 2.4 shows that the graphene sheets were packed densely by TiO<sub>2</sub> with average size of 31nm.

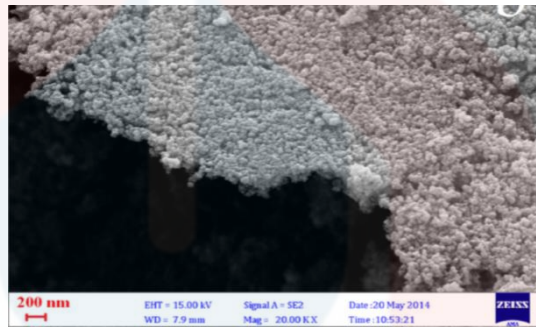


**Figure 2.4:** SEM image of 3% TG (Zargari *et al.*, 2016)

However, Al<sub>2</sub>O<sub>3</sub>-graphene nanocomposite has not yet been reported in the past research to manipulate its potential to become a substitute for the commonly used nanocomposites for photocatalytic degradation of dyed water.

## 2.4 Fabrication Methods

There are two common ways to reinforce graphene in the ceramic matrix which are powder processing and colloidal processing routes (Tatarko *et al.*, 2013). The other is sol-gel method which uses chemicals in synthesising the nanocomposites. However, in this study, hydrothermal method is conducted to

produce  $\text{Al}_2\text{O}_3$ -graphene nanocomposite. Figure 2.5 shows the overview of graphene ceramic matrix composite synthesis methods or processes that are commonly used.

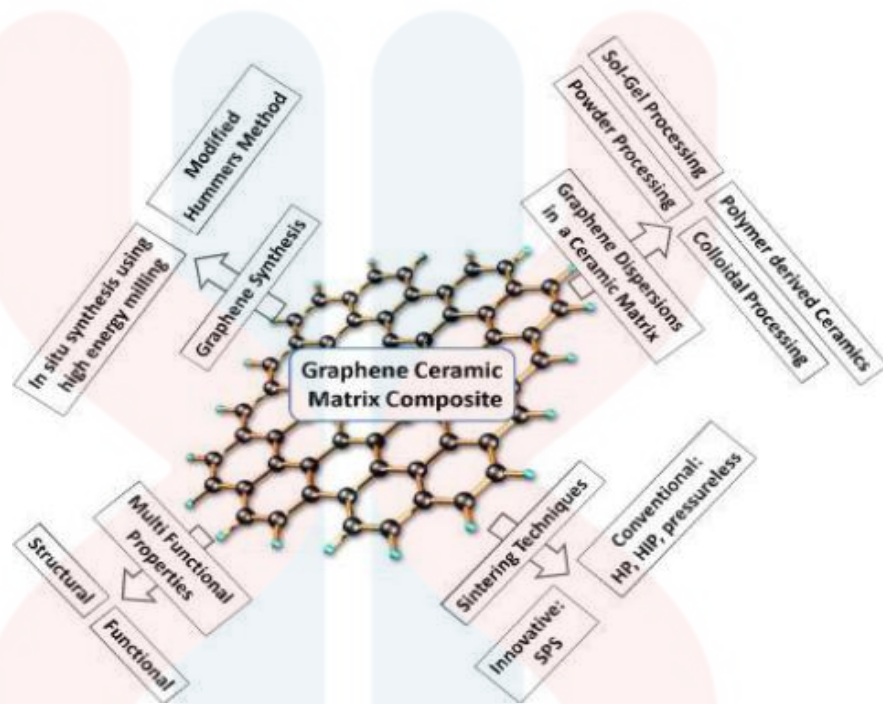


**Figure 2.5:** Overview for graphene synthesis methods (Porwal *et al.*, 2013).

### 2.4.1 Powder Processing

The powder processing is widely used in the research compared to colloidal processing even though the colloidal processing brings better dispersion of graphene in ceramic matrix (Porwal *et al.*, 2013). Powder processing is an easier route to graphene material as it is easier to process in this method compared to CNT in order to produce well-dispersed composites and it is also easier to scaled up (Porwal *et al.*, 2013). However, the method is expensive and not eco-friendly. Figure 2.6 shows the process of conventional powder processing route to produce  $\text{Al}_2\text{O}_3$ -SiC nanocomposite.

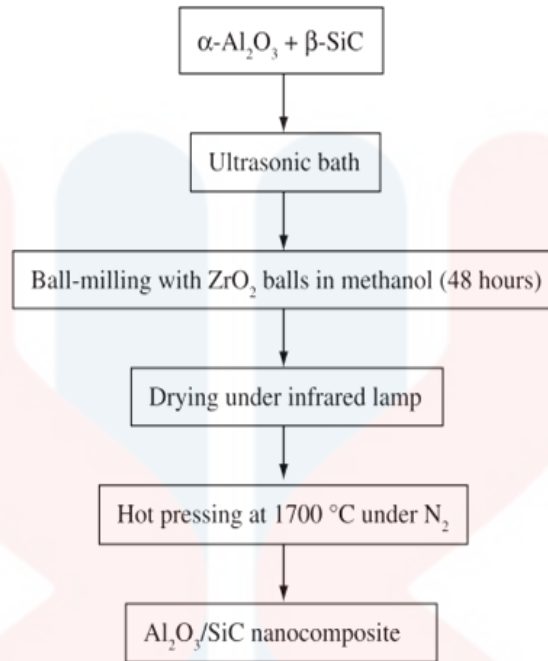


**Figure 2.6:** Conventional powder processing of  $\text{Al}_2\text{O}_3\text{-SiC}$  nanocomposite (Camargo *et al.*, 2009)

#### 2.4.2 Colloidal Processing

Porwal *et al.*, (2013) stated that colloidal processing is method to produce ceramic suspensions with the colloidal chemistry basis. This method is used to synthesize graphene-ceramic mixtures by dispersing colloidal suspensions of graphene in ceramic powders. The suspensions are mixed slowly by magnetic stirring or ultrasonication to aid the uniform dispersion of graphene into the matrix.

This method requires surface modification of graphene and matrix. Such modification involved the generation of opposite electric charges between ceramic particles and graphene. Through the modification of surface charges on ceramic and graphene powders, the degree of dispersion can be enhanced and resulted to a better quality dispersion of graphene (Porwal *et al.*, 2013). The research conducted by Gonzaleza *et al.*, (2015) showed that using colloidal method the aggregates of the graphene platelets are well dispersed in alumina composites.

### 2.4.3 Sol-gel Method

A review by Porwal *et al.*, (2013) stated that this method is required to create a precursor which undergoes condensation process to produce a green body with well-dispersed graphene. A stable suspension of well-dispersed graphene need to be prepared first where tetramethyl orthosilicate (TMOS) is added and undergoes sonication which provides uniform dispersed sol. A catalyst such as acidic water is added to introduce gelation where hydrolysis is performed. The composite gels are synthesized after go through condensation at room temperature. This technique is commonly used to synthesize silica nanocomposite.

Sol-gel method also offers a simple and inexpensive technique to produce high quality of thin films as compared to the plasma-enhanced chemical vapour deposition (PECVD) (Jannat *et al.*, 2016). A study made by Jannat *et al.*, (2016) investigated the deposition of single layer SiC-SiO<sub>2</sub> nanocomposite film as AR coating on Si solar cell using sol-gel precursor by spin coating followed by annealing at 450°C. The spin coating of sol-gel precursor has ability to deposit AR in large substrate and also in inexpensive way.

However, the disadvantages of sol-gel method are there is a possibility to have a drying problem that can slow the progress of fabricating bulk components, need a long processing time for gelation and drying process and also the need to use flammable solvents as catalysts (Porwal *et al.*, 2013).

### 2.4.4 Hydrothermal Method

Alternatively, hydrothermal method can be used to produce Al<sub>2</sub>O<sub>3</sub>-graphene nanocomposite. Hydrothermal synthesis is a method using temperature and pressure to produce crystal from aqueous solution usually in an autoclave. Su *et al.* (2016)

stated that hydrothermal route making the synthesising process is easier as this method can control particle morphology, phase composition, particle size and microstructures of the nanocomposites. This method commonly used in producing electrode for capacitor (Zhou *et al.*, 2014) as it will improves photocatalytic activity in water (Liu *et al.*, 2014), magnetic properties (Sobhani & Niasari, 2014) and electrical conductivity (Low *et al.*, 2015).

Compared to the conventional methods which are powder processing, colloidal processing and sol-gel method, this method is simpler (Yang *et al.*, 2015), more facile (Chang *et al.*, 2015) and eco friendly (Ezeigwe *et al.*, 2015). Latest research by Lam *et al.*, (2016) used green hydrothermal method to fabricate ZnO nanorods which involved no organic solvent or surfactant.

## **2.5 Nanocomposite for waste water application**

In wastewater application, textile industry is known for using dyes which are contaminants in water. Khandare *et al.*, (2015) stated that manufacturing and processing textile dye industries are one of the turbulent contaminators of water and soil. The textile effluents may have high concentration of dyestuffs, salts, acids, bases, surfactants, dispersants, humectants, oxidants and detergents making this water contaminated. The contaminated water needed to be cleaned for later consumption as this contaminant is harmful to human and environment (Belpaire *et al.*, 2015).

## **2.6 Degradation of dyes in water**

Textile dyes are known as mutagens and carcinogens as this will risk the ecosystems, animals and agriculture (Saratale *et al.*, 2011). Examples of dyes that commonly used in industry are MO, methylene blue (MB), rhodamine B (RhB) and

other synthetic dyestuffs (Lam *et al.*, 2016). Among the commonly used dyes, MO is one of the toxic and carcinogenic dyes that have been used in various applications and need to be removed from the waste water as it harmful to human and environment. Hence, it is necessary to choose the best material that has the best properties to be applied in wastewater treatment to degrade the toxic dyes.

Aware of this risk, many solutions has risen to remediate the dye containing effluents that are physical and biological adsorption, membrane filtration, oxidation, ozonation and also microbial biodegradation (Khandare *et al.*, 2015). Other technique is photocatalytic degradation as a technique to destroy organic pollutants in water.

## **2.7 Photocatalytic degradation using nanocomposite**

Nanocomposite has been used in the wastewater application generally in degradation contaminants and dyes. For the salt removal performance, Lai *et al.*, (2016) successfully made a novel thin film nanocomposite (TFN) membrane by reinforcing graphene oxide (GO) at different quantity into polysulfone (PSf) microporous substrate. After test was carried out, it was found that TFN membrane with 0.3wt% of GO possesses the highest water permeability with rejections for Na<sub>2</sub>SO<sub>4</sub> at 95.2%, MgSO<sub>4</sub> at 91.1%, MgCl at 62.1% and NaCl at 59.5% with respect to pure water.

Photocatalytic degradation is a process of generation of electron-hole pair under ultraviolet (UV) light which permits decomposition of organic pollutant (Leonard *et al.*, 2016). In environmental application, the photocatalytic degradation often used as to dissolve the unwanted substances generally in wastewater application. Figure 2.7 shows the process of degradation of MO in visible light.

The process of erasing dying wastewater using photocatalytic materials in nanocomposites has been increasingly interest in textile waste treatment.

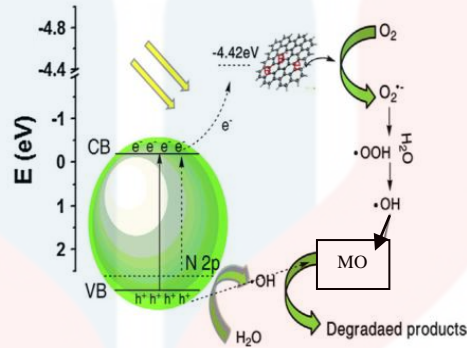


**Figure 2.7:** Visible light-energized photocatalytic degradation of MO (Hua *et al.*, 2015)

Research by Liu *et al.*, (2014) reviewed that  $\text{TiO}_2$ -based CNT has ability to perform in wastewater treatment as CNT exhibits high surface area, high stability and excellent photocatalytic activity in degradation of MO. Chaker *et al.*, (2016) found out that 0.5wt% of silver doped mesoporous  $\text{TiO}_2$  catalysts ( $\text{Ag}/\text{TiO}_2$ ) possess the highest photocatalytic degradation of MO in wastewater and also very stable even after three cycles of reuse. This make CNT and  $\text{TiO}_2$  become more potential as catalysts in waste water treatment. The latest material to evaluate its potential in photocatalytic degradation of MO for environmental application is graphene (Liu *et al.*, 2015; Choudhury *et al.*, 2014; Ahmad *et al.*, 2014).

Band gap energy in the material is important as this will ensure the low or high photocatalytic activity property for the material. Band gap is considered as energy level of the electron to go to the excited level. The energy band diagram is shown in Figure 2.8. The lower the bands gap will produce the higher the photocatalytic activity. It is a fact that spectral wavelength of visible light between



400 and 700 nm is considered for about 45% of the total energy of the solar radiation and UV light need about 10% only (Liao *et al.*, 2006).

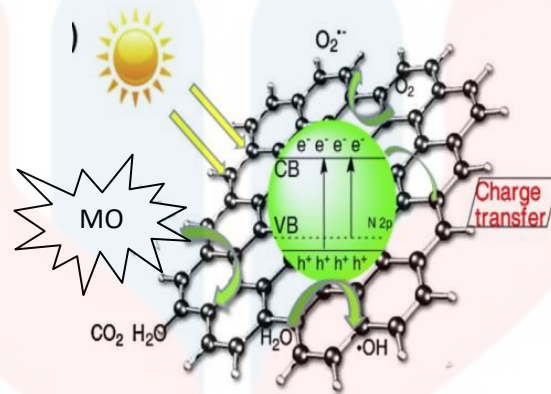


**Figure 2.8:** Energy band diagram (Hua *et al.*, 2015)

Among the catalysts, ZnO and TiO<sub>2</sub> materials are commonly used as semiconductors that possess high photosensitivity, low cost and eco-friendly (Wu *et al.*, 2006). However, these catalysts have large band gap energy that result the equal to or less than 385 nm only the wavelength for the both semiconductors to excite for photocatalytic uses under UV light illumination (Ozturk *et al.*, 2016). There are two common methods that are used to increase the photocatalytic activities which are to introducing dopants into the matrix lattice and to form coupled photocatalysts materials.

However, the recent research studies has never synthesised Al<sub>2</sub>O<sub>3</sub>-graphene nanocomposite to analyse its photocatalytic activity for the use in environmental application. Hence, the uniqueness of this study is to prove the capability of Al<sub>2</sub>O<sub>3</sub>-graphene nanocomposite for the photocatalytic absorption of MO to be used in environmental application.

## CHAPTER 3

### MATERIALS AND METHODS

#### 3.1 Introduction

This research was conducted using two parts which were preparation and characterization and performance study on Al<sub>2</sub>O<sub>3</sub>-graphene nanocomposite in absorbance of methyl orange. The overall work in this study is shown in Figure 3.1.

#### 3.2 Materials

The raw materials used in this study were graphene powder (>99% purity, average particle size >20 nm) and Al<sub>2</sub>O<sub>3</sub> powder (>99.9% purity, average particle size >20 µm) and were purchased by Sigma Aldrich.

#### 3.3 Preparation of Al<sub>2</sub>O<sub>3</sub>-graphene nanocomposite

Al<sub>2</sub>O<sub>3</sub> and graphene nanocomposite was prepared according to Table 3.1 using rule of mixture. Prior to performing hydrothermal method, the sample was premixed using ball milling for an hour. Then, 100 ml aqueous solution consists of 1M NaOH and water will be added to the mixture. The mixture will be stirred for 30 minutes and subjected to hydrothermal treatment at 200°C for 24 h in an autoclave. Then, the sample was washed with 200 ml HCl (0.1 M) and distilled water. The sample was dried in oven at 80°C for 24 hours.

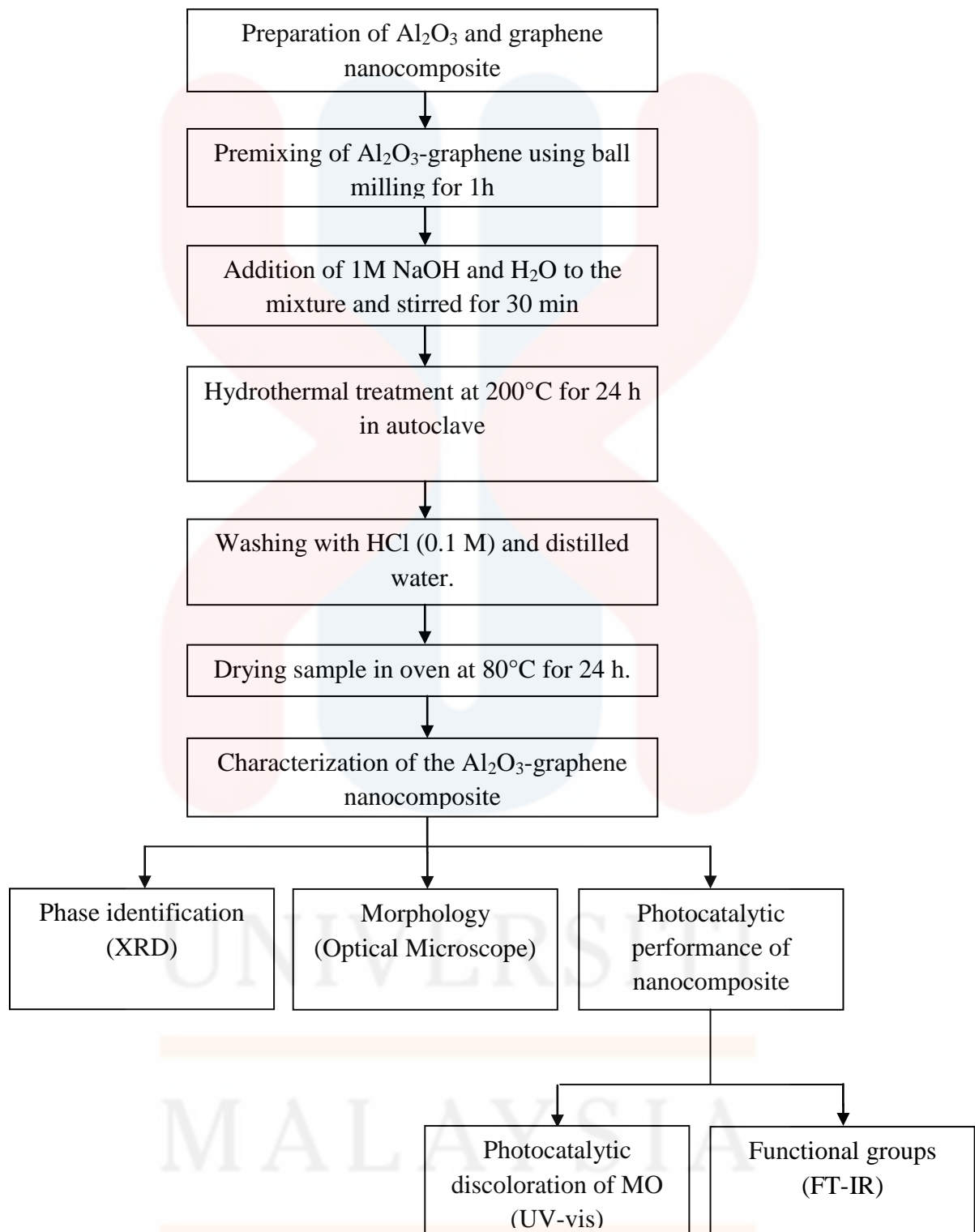


**Figure 3.1:** Flow chart of the research

**Table 3.1:** Composition of Al<sub>2</sub>O<sub>3</sub> and graphene to produce nanocomposites

Nanocomposite	Al <sub>2</sub> O <sub>3</sub> powder (wt%)	Graphene powder (wt%)
AG80	80	20
AG70	70	30
AG60	60	40
AG50	50	50
A100	100	0

### 3.4 Characterization of Al<sub>2</sub>O<sub>3</sub>-graphene nanocomposite

#### 3.4.1 Phase identification

The determination of phase identification of Al<sub>2</sub>O<sub>3</sub>-graphene nanocomposite was performed by X-Ray Diffraction (XRD) using Bruker D2 Phaser. The step size was 0.02° and the range of 2θ angle is between 20° to 80°. DIFFRAC-EVA software was used for qualitative analysis.

#### 3.4.2 Crystallite size and internal strain

Crystallite size and internal strain of Al<sub>2</sub>O<sub>3</sub>-graphene nanocomposite was determined by Williamson-Hall (WH) plot. The simplification of Williamson and Hall plot is as shown in Eq. (3.1) (Mote *et al.*, 2012) :-

$$\beta_{\text{tot}} \cos\theta = C\varepsilon \sin\theta + \frac{K\lambda}{L} \quad (3.1)$$

$$y = mx + c \quad (3.2)$$

The Eq. (3.1) is compared with the standard equation of a straight line ( $m =$  slope and  $c =$  intercept) shown in Eq. (3.2). The strain component can be obtained from the slope ( $C\varepsilon$ ) and the crystallite size from the intercept ( $K\lambda/L$ ) by plotting  $\beta_{\text{tot}} \cos\theta$  against  $\sin\theta$ .

### 3.4.3 Morphology

Jenoptik Metallurgical microscope of model MT8100 was used to obtain the morphology of  $\text{Al}_2\text{O}_3$ -graphene nanocomposite. The magnification of 20X was used in this analysis. The software ProgRes® CT3 was used to analyse the morphology of  $\text{Al}_2\text{O}_3$ -graphene nanocomposite.

### 3.4.4 Functional group

Fourier Transformation Infrared Spectrophotometer (FTIR) was used to determine the specific functional groups of  $\text{Al}_2\text{O}_3$ -graphene nanocomposite using Nicolet IS5 Spectrometer. Thermo Scientific OMNIC Spectra software was used to analyse the sample. This is to identify the structure of crystallized phases and to observe possible structural changes after doping the graphene in the  $\text{Al}_2\text{O}_3$  matrix.

### 3.4.5 Photocatalytic performance

The performance of nanocomposite on photocatalytic degradation of MO was studied. 0.1 g of samples was added into 100ml of 20 ppm MP dye solution. The aqueous suspension was magnetically stirred throughout the experiment. The suspension was subjected to visible light irradiation start from 1, 2, 3 and 4 h and any discoloration will be recorded by UV-vis.

UV-Vis spectrometer HACR DR 5000 with specification wavelength range of 190 to 1100 nm, accuracy of  $\pm 1$  nm in wavelength range 200 to 900 nm and resolution of 0.1 nm will be used to record the absorption spectra of the sample. In this analysis, the wavelength used was 457 nm and the original absorbance value of MO was 1.9. The percentage of the MO degradation will be calculated using the Eq. (3.3).

$$\text{MO absorption (\%)} = \frac{A_0 - A_1}{A_0} \times 100 \quad (3.3)$$

Where  $A_0$  is original absorbance value of MO and  $A_1$  is absorbance value of compositions with MO.

## CHAPTER 4

### RESULTS AND DISCUSSION

#### 4.1 Phase identification

Phase identification of raw materials and Al<sub>2</sub>O<sub>3</sub> doped graphene nanocomposite was characterized using XRD as shown in Figure 4.1. Peak pattern of raw Al<sub>2</sub>O<sub>3</sub> and after hydrothermal process shows no significant difference between these two patterns. This is because at temperature set up 200°C of hydrothermal was not enough to form new or change structure in Al<sub>2</sub>O<sub>3</sub>. This is in agreement with the previous report done by Shehata *et al.*, (2011), that even though at thermal treatment of 975°C could not change Al<sub>2</sub>O<sub>3</sub> form as the Al<sub>2</sub>O<sub>3</sub> were uniformly dispersed.

In Al<sub>2</sub>O<sub>3</sub>-graphene nanocomposite, the intensity of Al<sub>2</sub>O<sub>3</sub> become sharp with decreasing graphene content indicating this composite is a polycrystalline material. While, peak of graphene was maintained since the amount graphene was higher. In the nanocomposite containing higher Al<sub>2</sub>O<sub>3</sub> content, small shift to the right can be detected indicating the presence of graphene affects the structure of Al<sub>2</sub>O<sub>3</sub>.

Moreover, as the Al<sub>2</sub>O<sub>3</sub> content increased, the crystal structure of the nanocomposites also changes. The intensity of Al<sub>2</sub>O<sub>3</sub> becomes narrower which is due to hexagonal lattice of graphene changes to tetragonal after it is dispersed in Al<sub>2</sub>O<sub>3</sub>. This indicates that the introduction of graphene to the Al<sub>2</sub>O<sub>3</sub> matrix changed the crystal structure of the nanocomposite.

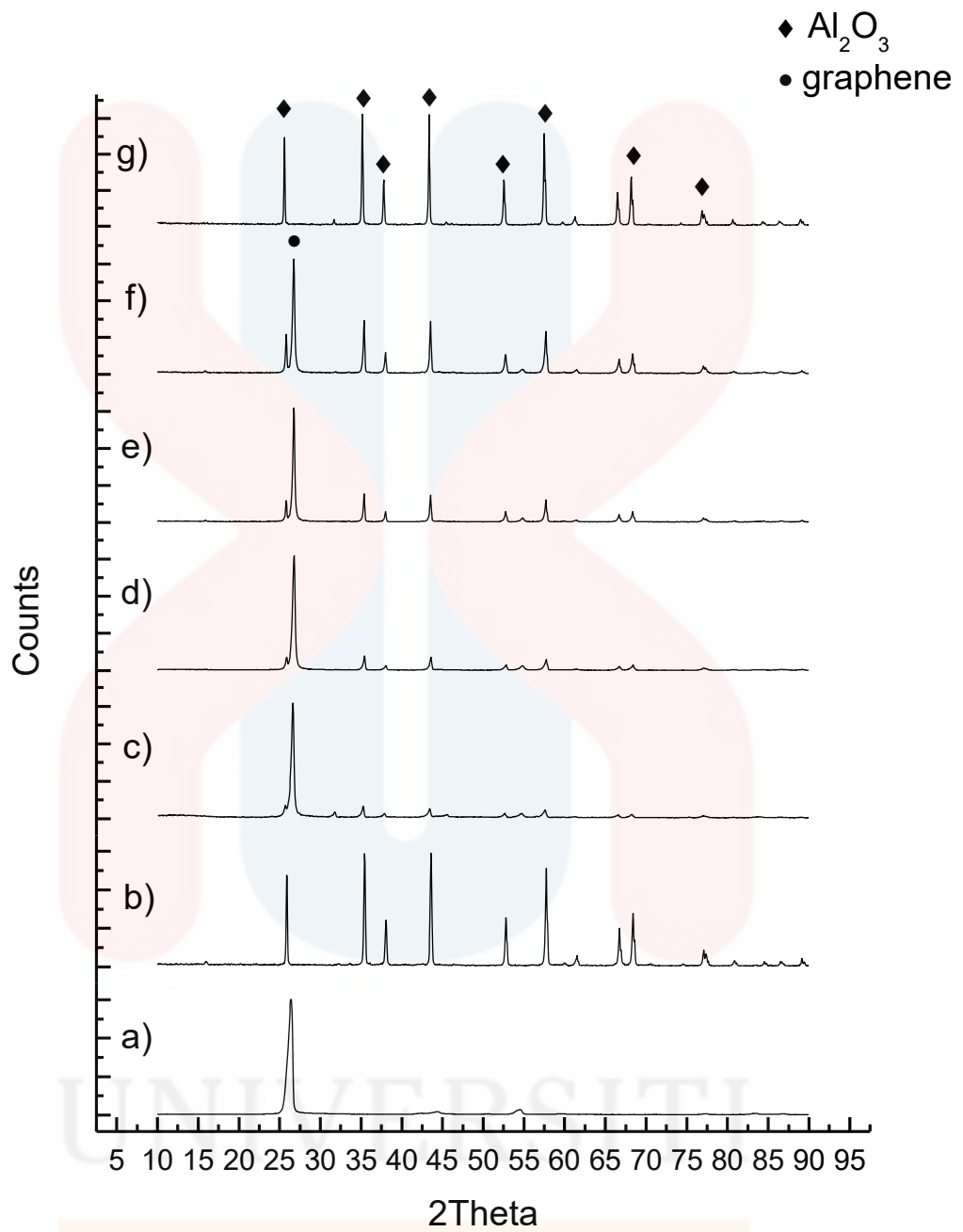


**Figure 4.1:** XRD patterns of pure a) graphene and b)  $\text{Al}_2\text{O}_3$  with the compositions c) AG50, d) AG60, e) AG70 and f) AG80 and g) A100



### 4.2 Crystallite size and internal strain

The plot of  $B_r \cos \theta$  against  $\sin \theta$  is shown in the Figure 4.2. This plot was used to calculate the crystallite size and internal strain of  $\text{Al}_2\text{O}_3$ -graphene nanocomposite. Broadening peaks (2-1-1) and (0-1-1) for the  $\text{Al}_2\text{O}_3$  was drawn in straight line with negative slope and intercept (Mote *et al.*, 2012). The calculated crystallite size and internal strain was presented in Table 4.3. It can be observed that as the graphene content decreased, the crystallite size of  $\text{Al}_2\text{O}_3$  decreased and the internal strain increased. Sathyaseelan *et al.*, (2013) reported that when the reinforcing phase content decreased, the crystallite size of  $\text{Al}_2\text{O}_3$  increased.

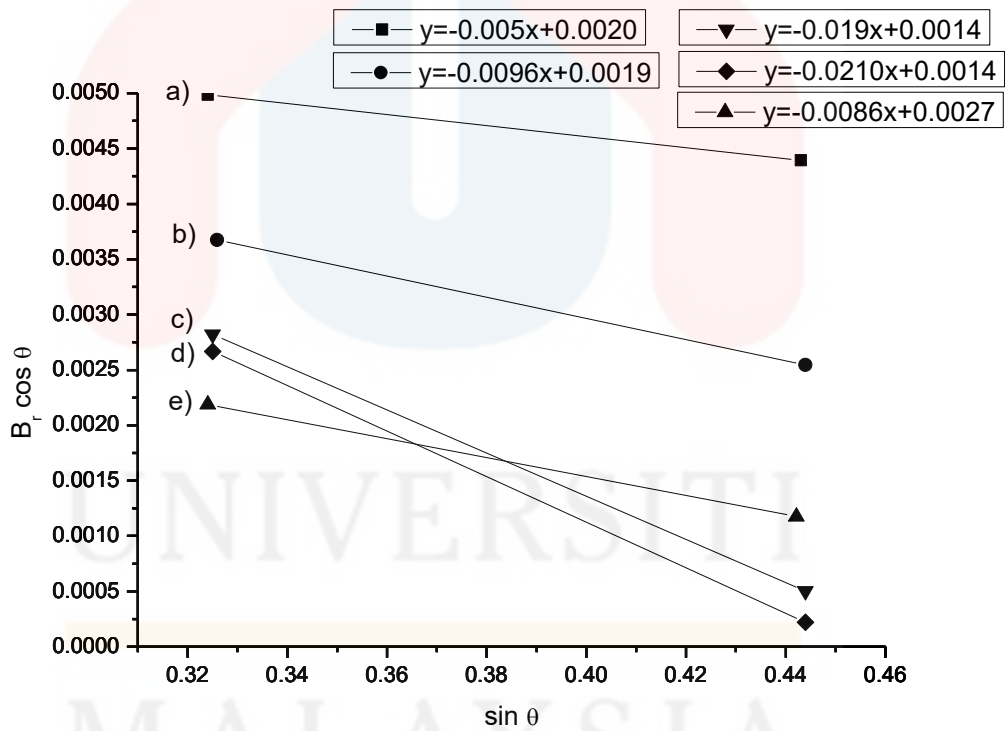


**Figure 4.2:** Plot of  $B_r \cos \theta$  against  $\sin \theta$  in a) AG50, b) AG60, c) AG70, d) AG80 and e) A100

**Table 4.1:** The crystallite size and internal strain of Al<sub>2</sub>O<sub>3</sub>-graphene nanocomposite

Sample	Crystallite size (nm)	Internal strain
AG50	20.3	0.0050
AG60	19.0	0.0096
AG70	14.6	0.0195
AG80	14.3	0.0206
A100	27.0	0.0086

### 4.3 Morphology

The morphology of Al<sub>2</sub>O<sub>3</sub>-graphene nanocomposite was studied from the optical microscope images. Figure 4.3 shows the optical images of raw Al<sub>2</sub>O<sub>3</sub> and graphene before the hydrothermal process. Small size of Al<sub>2</sub>O<sub>3</sub> and large size of graphene particles could be observed.

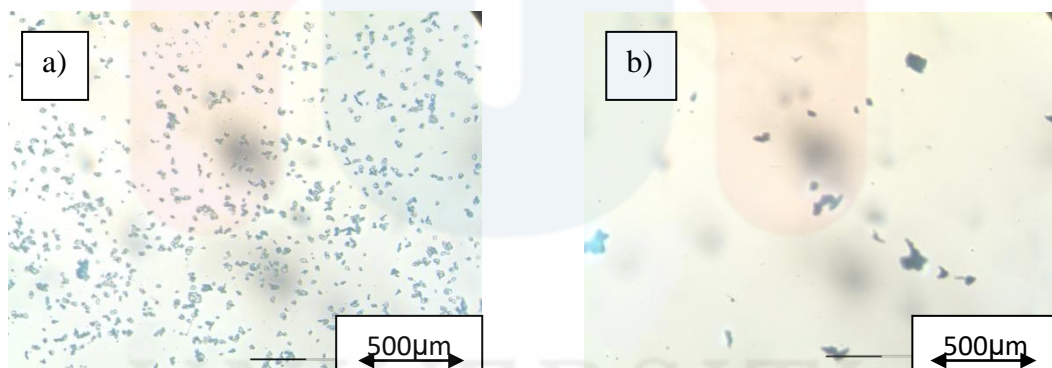


**Figure 4.3:** The optical images of pure a) Al<sub>2</sub>O<sub>3</sub> and b) graphene before hydrothermal process

Figure 4.4 shows Al<sub>2</sub>O<sub>3</sub> and Al<sub>2</sub>O<sub>3</sub> doped graphene nanocomposites after hydrothermal process. The particle size of Al<sub>2</sub>O<sub>3</sub> and graphene become larger after hydrothermal process as a result of the change of an inhomogeneous over time such that small crystals dissolve and redeposit onto larger crystal. This phenomenon is called Ostwald ripening (Voorhees, 1985). Meanwhile, optical image of equal composition of Al<sub>2</sub>O<sub>3</sub> and graphene exhibited small particle size compared to that of higher content of Al<sub>2</sub>O<sub>3</sub>. This is due to the highest composition of graphene with the

lowest content of  $\text{Al}_2\text{O}_3$  made it small in particle size compared to the higher composition of  $\text{Al}_2\text{O}_3$  which leads to the larger particle size of  $\text{Al}_2\text{O}_3$ -graphene nanocomposite.

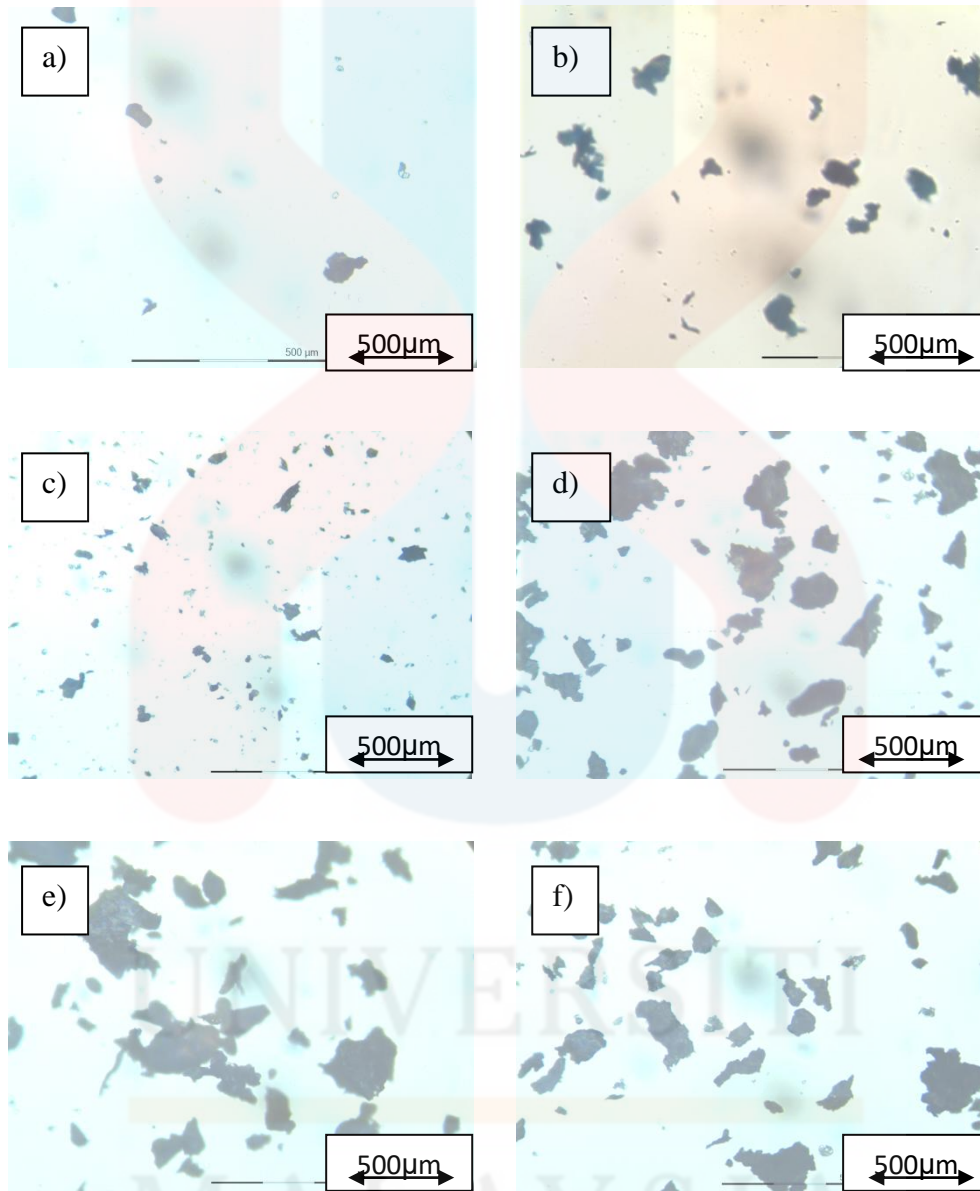


**Figure 4.4:** The optical images of a) A100, b) G100, c) AG50, d) AG60, e) AG70 and f) AG80 after hydrothermal process

#### 4.4 Functional group

Figure 4.5 presents the FTIR spectra of raw  $\text{Al}_2\text{O}_3$  and graphene and hydrothermally synthesized  $\text{Al}_2\text{O}_3$ -graphene nanocomposite. The significant

absorption peak located at 1850 to 2250  $\text{cm}^{-1}$  is observed which similar broad peak absorption at 2104  $\text{cm}^{-1}$  with pure graphene which corresponding to the triple bond of carbon stretching vibrations.  $\text{Al}_2\text{O}_3$  also possess this peak absorption but in shallower peak. Moreover, other peak absorptions are observed at 3291 and 3378  $\text{cm}^{-1}$  attributed to the OH vibrations of adsorbed water molecules (Yang *et al.*, 2015; Muthumari *et al.*, 2015; Han *et al.*, 2016). When comparing the spectrum of raw  $\text{Al}_2\text{O}_3$  and A100, the peak absorption of 3378  $\text{cm}^{-1}$  was not seen in raw  $\text{Al}_2\text{O}_3$ . This could be explained that after hydrothermal process, the OH bond was developed inside the  $\text{Al}_2\text{O}_3$  particles.

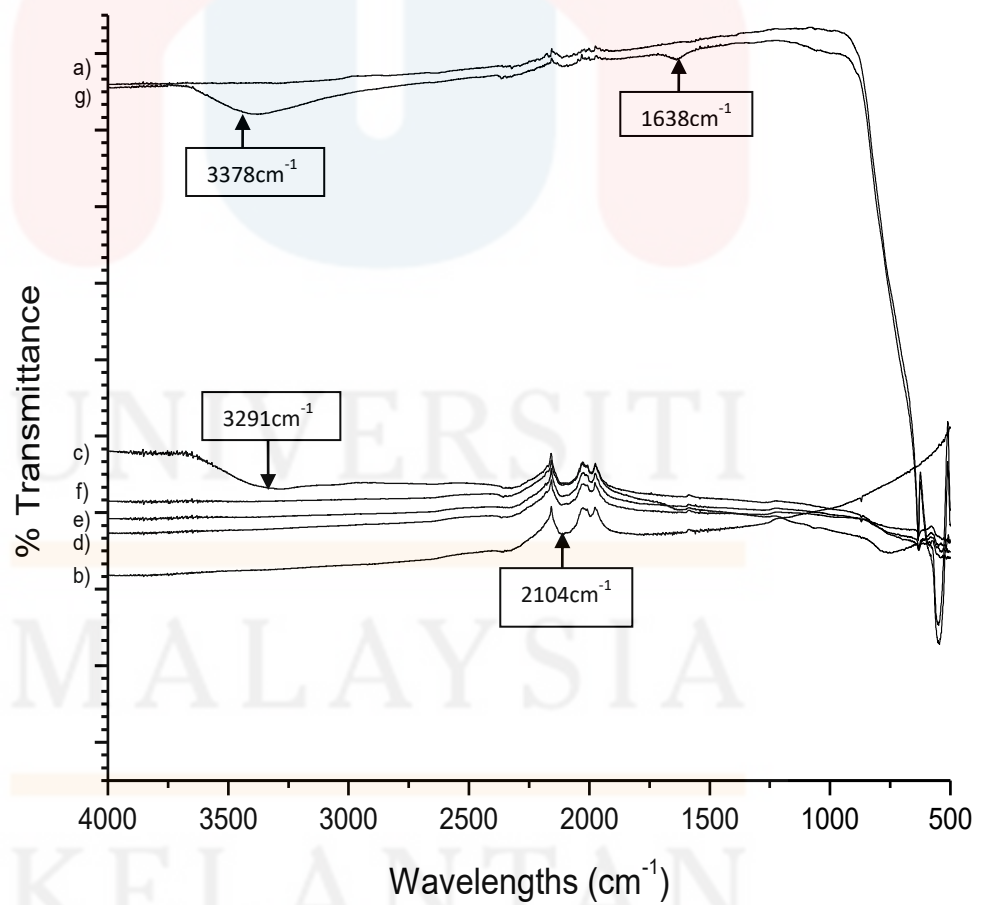


**Figure 4.5:** FTIR spectra of pure a)  $\text{Al}_2\text{O}_3$ , b) graphene with the compositions c) AG50, d) AG60, e) AG70, f) AG80 and g) A100.

The peak absorption at  $1638\text{ cm}^{-1}$  was observed in A100 is belong to amide group stretching vibration, however, not present in the raw  $\text{Al}_2\text{O}_3$  spectrum. The peak was also present after the hydrothermal process of  $\text{Al}_2\text{O}_3$ . Furthermore, the percentage transmittance of  $\text{Al}_2\text{O}_3$  and graphene was quite further from each other. This means that the intensity of  $\text{Al}_2\text{O}_3$  is greater than graphene because  $\text{Al}_2\text{O}_3$  absorbed more amount of radiation than graphene (Kloprogge *et al.*, 2002).

#### 4.5 Absorption of MO dye

The performance of  $\text{Al}_2\text{O}_3$ -graphene nanocomposite on percentage of MO absorption in visible light is given in Figure 4.6. From the result, it can be observed that as the  $\text{Al}_2\text{O}_3$  content became higher, the absorbance of MO became higher. The two highest percentages of MO absorption are AG60 and AG80 with more than 80%. This showed that the photocatalytic efficiencies of  $\text{Al}_2\text{O}_3$ -graphene nanocomposite were influenced by the introduction of graphene as proven by Yan *et al.*, 2013.

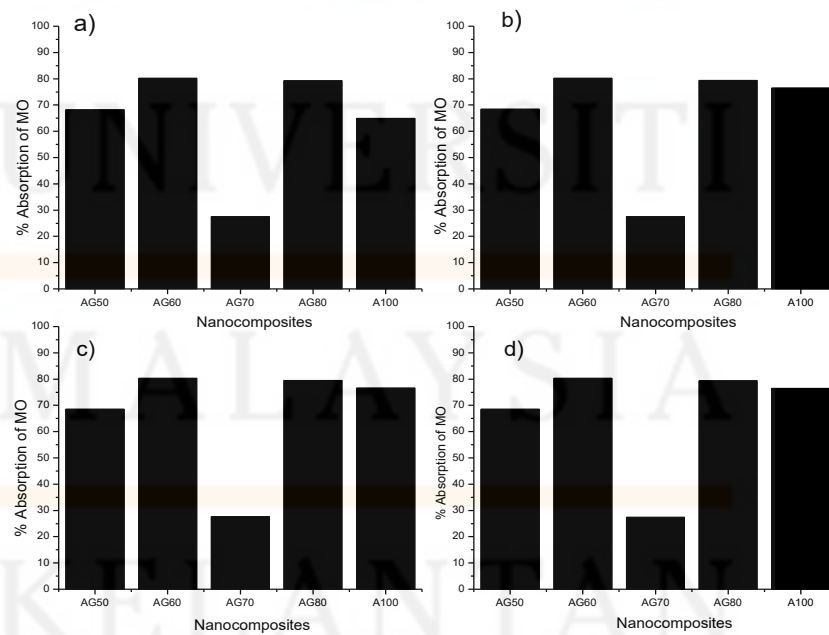


**Figure 4.6:** The percentage of absorption of MO for a) 1 b) 2 c) 3 and d) 4 h

It can be seen that AG70 absorbed just about 30% of MO. This error in the result might be caused by the technical error that occurred at the synthesising process of the nanocomposites.

A100 also absorbed MO better with slightly increased percentage in 4 h. This is the same result as reported by Li *et al.*, (2007) that Al<sub>2</sub>O<sub>3</sub> itself also better in degradation of MO. In the first 3h, the MO absorption of all the compositions has increased but after that began to decrease gradually. This might due to the surrounding environment factor that could affect the reading such as light intensity and temperature.

## CHAPTER 5

### CONCLUSION AND RECOMMENDATION

#### 5.1 CONCLUSION

$\text{Al}_2\text{O}_3$ -graphene nanocomposite was successfully synthesized using hydrothermal method. The characterization of the  $\text{Al}_2\text{O}_3$ -graphene nanocomposite was carried out using XRD, FTIR and Optical images. Several characterizations can be concluding as follows:

1. The introduction of graphene changes the internal structure of  $\text{Al}_2\text{O}_3$  due to the small shift to the right in the diffraction peak pattern.
2.  $\text{Al}_2\text{O}_3$ -graphene nanocomposite is considered as polycrystalline material as the intensity of  $\text{Al}_2\text{O}_3$  became sharp with decreasing graphene content.
3. Crystallite size of  $\text{Al}_2\text{O}_3$  reduced and internal strain increased with decreasing graphene content.
4. The morphology of  $\text{Al}_2\text{O}_3$ -graphene nanocomposite was significantly influenced by the hydrothermal condition.
5. The increased of  $\text{Al}_2\text{O}_3$  content demonstrate better in absorption of MO.
6. It was found that  $\text{Al}_2\text{O}_3$ -20wt% graphene nanocomposite performed the best in absorption of MO dye which made  $\text{Al}_2\text{O}_3$ -graphene nanocomposite is a potential candidate for environmental application.

## 5.2 RECOMMENDATION

For the future work, it is recommended to use SEM instead of OM to analyse the morphology of Al<sub>2</sub>O<sub>3</sub>-graphene nanocomposite. This is because SEM provides higher resolution than OM which makes it possible to watch the morphology in more detail. The structure of graphene embedded well inside the Al<sub>2</sub>O<sub>3</sub> can also be seen clearly with the use of SEM.

Moreover, different temperature of hydrothermal synthesis can be explored for a longer duration of time. With this parameter, it is possible to demonstrate the best temperature for the Al<sub>2</sub>O<sub>3</sub>-graphene nanocomposite could perform in absorption of MO dye.

Other test that needs to carry out is photocatalytic activity of Al<sub>2</sub>O<sub>3</sub>-graphene towards MO dye. This test includes the calculation of band gap of the nanocomposite which can be compared with the previous reports. Furthermore, the absorption wavelength of MO can be obtained through this test which can be important in determining the suitable photocatalyst content for the future work.



## REFERENCES

- Bai, H., Zan, X., Zhang, L., & Sun, D. D. (2015). Multi-functional CNT/ZnO/TiO<sub>2</sub> nanocomposite membrane for concurrent filtration and photocatalytic degradation. *Separation and Purification Technology*, 156, 922-930.
- Belpaire, C., Reyns, T., Geeraerts, C., & Loco, J. V. (2015). Toxic textile dyes accumulate in wild European eel *Anguilla anguilla*. *Chemosphere*, 138, 784-791.
- Camargo, P. H. C., Satyanarayana, K. G., & Wypych, F. (2009). Nanocomposites: Synthesis, Structure, Properties and New Application Opportunities. *Materials Research*, 12, 1-39.
- Centeno, A., Rocha, V. G., Alonso, B., Fernández, A., Gutierrez-Gonzalez, C. F., Torrecillas, R., & Zurutuza, A. (2013). Graphene for tough and electroconductive alumina ceramics. *European Ceramic Society*, 33, 3201-3210.
- Chaker, H., Chérif-Aouali, L., Khaoulani, S., Bengueddach, A., & Fourmentin, S. (2016). Photocatalytic degradation of methyl orange and real wastewater by silver doped mesoporous TiO<sub>2</sub> catalysts. *Journal of Photochemistry and Photobiology A: Chemistry*, 318, 142-149.
- Chen, D., Zou, L., Li, S., & Zheng, F. (2016). Nanospherical like reduced graphene oxide decorated TiO<sub>2</sub> nanoparticles: an advanced catalyst for the hydrogen evolution reaction. *Sci Rep*, 6, 20335.
- Chen, F., Ying, J., Wang, Y., Du, S., Liu, Z., & Huang, Q. (2016). Effects of graphene content on the microstructure and properties of copper matrix composites. *Carbon*, 96, 836-842.
- Chen, G., Sun, M., Wei, Q., Zhang, Y., Zhu, B., & Du, B. (2013). Ag<sub>3</sub>PO<sub>4</sub>/graphene-oxide composite with remarkably enhanced visible-light-driven photocatalytic activity toward dyes in water. *Journal of Hazardous Materials*, 244-245, 86-93.
- Chinelatto, A. S. A., Chinelatto, A. L., Ojaimi, C. L., Ferreira, J. A., & Pallone, E. M. (2014). Effect of sintering curves on the microstructure of alumina-zirconia nanocomposites. *Ceramics International*, 40, 14669-14676.
- Davis K. (2010). Material Review: Alumina (Al<sub>2</sub>O<sub>3</sub>). *School of Doctoral Studies (European Union) Journal*, 109-114.
- Dong, Y. L., Xu, F. M., Shi, X. L., Zhang, C., Zhang, Z. J., Yang, J. M., & Tan, Y. (2009). Fabrication and mechanical properties of nano-/micro-sized Al<sub>2</sub>O<sub>3</sub>/SiC composites. *Materials Science and Engineering A*, 504, 49-54.
- Drakonakis, V. M., Aureli, M., Doumanidis, C. C., & Seferis, J. C. (2014). Modulus-density negative correlation for cnt-reinforced polymer nanocomposites: modeling and experiments. *Composites: Part B*, 70, 175-183.
- Durán-Álvarez, J. C., Avella, E., Ramírez-Zamora, R. M., & Zanella, R. (2016). Photocatalytic degradation of ciprofloxacin using mono- (Au, Ag and Cu) and bi- (Au-Ag and Au-Cu) metallic nanoparticles supported on TiO<sub>2</sub> under UV-C and simulated sunlight. *Catalysis Today*, 266, 175-187.
- Ezeigwe E. R., Tan M. T. T., Khiew P. S., & Siong C. W. (2015). One-step green synthesis of graphene/ZnO nanocomposites for electrochemical capacitors. *Ceramics International*, 41(1), 715-724.
- F. Han, H. Li, J. Yang, X. Cai, & Fu, L. (2016). One-pot synthesis of cuprous oxide-reduced graphene oxide nanocomposite with enhanced photocatalytic and electrocatalytic performance. *Physica E: Low-dimensional Systems and Nanostructures*, 77, 122-126.
- Ghaseminezhad, S. M., & Shojaosadati, S. A. (2016). Evaluation of the antibacterial activity of Ag/Fe<sub>3</sub>O<sub>4</sub> nanocomposites synthesized using starch. *Carbohydrate polymers*, 144, 454-463.
- Gutierrez-Gonzalez, C. F., Smirnov, A., Centeno, A., Fernández, A., Alonso, B., Rocha, V. G., Bartolome, J. F. (2015). Wear behavior of graphene/alumina composite. *Ceramics International*, 41, 7434-7438.
- Hanzel, O., Sedlacek, J., & Sajgalik, P. (2014). New approach for distribution of carbon nanotubes in alumina matrix. *European Ceramic Society*, 34, 1845-1851.
- Hua, Z., Zhang, X., Bai, X., Lv, L., Ye, Z., & Huang, X. (2015). Nitrogen-doped perovskite-type La<sub>2</sub>Ti<sub>2</sub>O<sub>7</sub> decorated on graphene composites exhibiting efficient photocatalytic activity toward bisphenol A in water. *Journal of Colloid and Interface Science*, 450, 45-53.
- Jannat, A., Lee, W., Akhtar, M. S., Li, Z. Y., & Yang, O.-B. (2016). Low Cost Sol-Gel derived SiC-SiO<sub>2</sub> Nanocomposite as Anti Reflection layer for Enhanced Performance of Crystalline Silicon Solar Cells. *Applied Surface Science*, 369, 545-551.
- Kim, H. J., Lee, C., Sung-Min, L., Yoon-Suk, O., Lim, Y. S., Yoon, D. H., Ruoff, R. S. (2014). Unoxidized Graphene/Alumina Nanocomposite: Fracture- and Wear-Resistance Effects of Graphene on Alumina Matrix. *Scientific Reports*, 4, 5176.

- Klopprogge, J. T., Ruan, H. D., & Frost, R. L. (2002). Thermal Decomposition Of Bauxite Minerals: Infrared Emission Spectroscopy Of Gibbsite, Boehmite And Diaspore. *Journal of Materials Science*, 37(6), 1121-1129.
- Lai, G. S., Lau, W. J., Goh, P. S., Ismail, A. F., Yusof, N., & Tan, Y. H. (2016). Graphene oxide incorporated thin film nanocomposite nanofiltration membrane for enhanced salt removal performance. *Desalination*, 387, 14-24.
- Lam, S.-M., Sin, J.-C., & Mohamed, A. R. (2016). Fabrication of ZnO nanorods via a green hydrothermal method and their light driven catalytic activity towards the erasure of phenol compounds. *Materials Letters*, 167, 141-144.
- Léonard, G. L.-M., Remy, S., & Heinrichs, B. (2016). Overview of superhydrophilic, photocatalytic and anticorrosive properties of TiO<sub>2</sub> thin films doped with multi-walled carbon nanotubes and deposited on 316L stainless steel. *Advances in Functional Materials*, 3(2), 434-438.
- Li, Q., Guo, B., Yu, J., Ran, J., Zhang, B., Yan, H., & Gong, J. R. (2011). Highly efficient visible-light-driven photocatalytic hydrogen production of CdS-cluster-decorated graphene nanosheets. *J Am Chem Soc*, 133(28), 10878-10884.
- Liu, J., Yang, Y., Hassinin, H., Jumbu, N., Deng, S., Zuo, Q., & Jiang, K. (2015). Graphene-Alumina Nanocomposites with Improved Mechanical Properties for Biomedical Applications. *ACS Applied Materials & Interfaces*, 8(4), 2607-2616.
- Liu, N., Chen, X., Zhang, J., & Schwank, J. W. (2014). A review on TiO<sub>2</sub>-based nanotubes synthesized via hydrothermal method: Formation mechanism, structure modification, and photocatalytic applications. *Catalysis Today*, 225, 34-51.
- Long, X., Bai, Y., Algarni, M., Choi, Y., & Chen, Q. (2015). Study on the strengthening mechanisms of Cu/CNT nano-composites. *Materials Science & Engineering A*, 645, 347-356.
- Low, S. S., Tan, M. T., Loh, H. S., Khiew, P. S., & Chiu, W. S. (2015). Facile hydrothermal growth graphene/ZnO nanocomposite for development of enhanced biosensor. *Anal Chim Acta*, 903, 131-141.
- Mote, V. D., Purushotham, Y., & Dole, B. N. (2012). Williamson-Hall analysis in estimation of lattice strain in nanometer-sized ZnO particles. *Journal of Theoretical and Applied Physics*, 6(1), 6.
- Muñoz-Fernandez, L., Sierra-Fernandez, A., Milošević, O., & Rabanal, M. E. (2016). Solvothermal synthesis of Ag/ZnO and Pt/ZnO nanocomposites and comparison of their photocatalytic behaviors on dyes degradation. *Advanced Powder Technology*, 27(3), 983-993.
- Muthumari, M., & P., T. (2015). Synthesis and Characterization of Mass production of high quality Reduced Graphene Sheets via a Chemical Method, *Graphene*, 3(2), 7-13.
- Nurzulaikha, R., Lim, H. N., Harrison, I., Lim, S. S., Pandikumar, A., Huang, N. M., Ibrahim, I. (2015). Graphene/SnO<sub>2</sub> nanocomposite-modified electrode for electrochemical detection of dopamine. *Sensing and Bio-Sensing Research*, 5, 42-49.
- Ozturk, B., & Soyulu, G. S. P. (2016). Promoting role of transition metal oxide on ZnTiO<sub>3</sub>-TiO<sub>2</sub> nanocomposites for the photocatalytic activity under solar light irradiation. *Ceramics International*, 42(9), 11184-11192.
- Porwal, H., Grasso, S., & Reece, M. J. (2013). Review of graphene-ceramic matrix composites. *Advances in Applied Ceramics*, 112(8), 443-454.
- Porwal, H., Kasiarova, M., Tatarko, P., Grasso, S., Dusza, J., & Reece, M. J. (2015). Scratch behaviour of graphene alumina nanocomposites. *Advances in Applied Ceramics*, 114, 34-41.
- Porwal, H., Tatarko, P., Grasso, S., Khaliq, J., Dlouhy, I., & Reece, M. J. (2013). Graphene reinforced alumina nano-composites. *Carbon*, 64, 359-369.
- Ramdani, N., Wang, J., Wang, H., Feng, T., Derradji, M., & Wen-bin, L. (2014). Mechanical and thermal properties of silicon nitride reinforced polybenzoxazine nanocomposites. *Composites Science and Technology*, 112(8), 443-454.
- Rutkowski, P., Dubiel, A., Klimczyk, P., Jaworska, L., & Stobierski, L. (2015). Thermal properties of pressure sintered alumina-graphene composites. *Springer*, 122(1), 105-114.
- Sathyaseelan, B., Baskaran, I., & Sivakumar, K. (2013). Phase Transition Behavior of Nanocrystalline Al<sub>2</sub>O<sub>3</sub> Powders. *Soft Nanoscience Letters*, 03(04), 69-74.
- Shehata, F., Abdelhameed, M., Fathy, A., & Elmahdy, M. (2011). Preparation and Characteristics of Cu-Al<sub>2</sub>O<sub>3</sub> Nanocomposite. *Open Journal of Metal*, 01(02), 25-33.
- Simões S., Viana F., Reis M. A.L., & Vieira M. F. (2015). Influence of dispersion/mixture time on mechanical properties of Al-CNTs nanocomposites. *Composite Structures*, 126, 114-122.
- Sobhani, A., & Salavati-Niasari, M. (2014). Hydrothermal synthesis, characterization, and magnetic properties of cubic MnSe<sub>2</sub>/Se nanocomposites material. *Journal of Alloys and Compounds*, 617, 93-101.

- Spanos, K. N., Georgantzinou, S. K., & Anifantis, N. K. (2015). Mechanical properties of graphene nanocomposites: A multiscale finite element prediction. *Composite Structures*, 132, 536-544.
- Su, C., Tseng, C.-M., Chen, L.-F., You, B.-H., Hsu, B.-C., & Chen, S.-S. (2006). Sol-hydrothermal preparation and photocatalysis of titanium dioxide. *Thin Solid Films*, 498, 259-265.
- Sze-Mun, L., Jin-Chung, S., & Mohamed, A. R. (2016). A review on photocatalytic application of g-C<sub>3</sub>N<sub>4</sub>/semiconductor (CNS) nanocomposites towards the erasure of dyeing wastewater. *Materials Science in Semiconductor Processing*, 47, 62-84.
- Tabandeh-Khorshid, M., Cho, K., Rohatgi, P. K., Ferguson, J. B., Schultz, B. F., & Chang-Soo, K. (2016). Strengthening mechanisms of graphene- and Al<sub>2</sub>O<sub>3</sub>-reinforced aluminum nanocomposites synthesized by roomtemperature milling. *Materials and Design*, 92, 79-87.
- Trunec M., Maca K., & Chmelik R. (2015). Polycrystalline alumina ceramics doped with nanoparticles for increased transparency. *Journal of the European Ceramic Society*, 35(3), 1001-1009.
- Voorhees, P. W. (1985). The theory of Ostwald ripening. *Journal of Statistical Physics*, 38(1), 231-252.
- Xie, B., Chen, Y., Yu, M., Sun, T., Lu, L., Xie, T., Wu, Y. (2016). Hydrothermal synthesis of layered molybdenum sulfide/N-doped graphene hybrid with enhanced supercapacitor performance. *Carbon*, 99, 35-42.
- Yan, J., Wang, K., Xu, H., Qian, J., Liu, W., Yang, X., & Li, H. (2013). Visible-light photocatalytic efficiencies and anti-photocorrosion behavior of CdS/graphene nanocomposites: Evaluation using methylene blue degradation. *Chinese Journal of Catalysis*, 34(10), 1876-1882.
- Yang, G. (2015). One-pot Preparation of Reduced Graphene Oxide/Silver Nanocomposite and Its Application in the Electrochemical Determination of 4-Nitrophenol. *Electrochemical Science*, 10, 9632-9640.
- Yazdani, B., Xia, Y., Ahmad, I., & Zhua, Y. (2014). Graphene and carbon nanotube (GNT)-reinforced alumina nanocomposites. *European Ceramic Society*, 35(1), 179-186.
- Yazdani, B., Xu, F., Ahmad, I., Hou, X., Xia, Y., & Zhu, Y. (2015). Tribological performance of Graphene/Carbon nanotube hybrid reinforced Al<sub>2</sub>O<sub>3</sub> composites. *Scientific Reports*, 5, 11579.
- Yoon, S.-D., Byun, H.-S., & Yun, Y.-H. (2015). Characterization and photocatalytic properties of ceramics TiO<sub>2</sub> nanocomposites. *Ceramics International*, 41(6), 8241-8246.
- Zargari, S., Rahimi, R., Ghaffarinejad, A., & Morsali, A. (2016). Enhanced visible light photocurrent response and photodegradation efficiency over TiO<sub>2</sub>-graphene nanocomposite pillared with tin porphyrin. *J Colloid Interface Sci*, 466, 310-321.
- Zhou, Z., Ni, H., & Li-Zhen, F. (2014). Hydrothermal Synthesis of Graphene/Nickel Oxide Nanocomposites Used as the Electrode for Supercapacitors. *Journal of Nanoscience and Nanotechnology*, 14(7), 4976-4981.

## APPENDIX A

### A.1 Williamson-Hall method

**Table A.1:** Williamson-Hall method

Sample No	hkl	2θ(Obs.Max)	θ	θ(rad)	cosθ	B(°)	B (rad)	B <sub>i</sub> (°)	B <sub>i</sub> (rad)	$B_r^2 = B^2 - B_i^2$	B <sub>r</sub> cosθ	sinθ	<D>	Strain
AG50	-22	52.59	26.295	0.459	0.896496	0.298	0.0052	0.1	0.0017	0.0049	0.0044	0.443052	0.0066	-0.0050
	0 -1 1	37.808	18.904	0.33	0.946042	0.318	0.0056	0.1	0.0017	0.0053	0.0050	0.324043	2.03E-08	-0.2487

Sample No	hkl	2θ(Obs.Max)	θ	θ(rad)	cosθ	B(°)	B (rad)	B <sub>i</sub> (°)	B <sub>i</sub> (rad)	$B_r^2 = B^2 - B_i^2$	B <sub>r</sub> cosθ	sinθ	<D>	Strain
AG60	-22	52.768	26.384	0.46	0.896052	0.191	0.0033	0.1	0.0017	0.0028	0.0025	0.443948	0.0068	-0.0096
	0 -1 1	38.026	19.013	0.332	0.945392	0.244	0.0043	0.1	0.0017	0.0039	0.0037	0.325934	1.97E-08	-0.4777

Sample No	hkl	2θ(Obs.Max)	θ	θ(rad)	cosθ	B(°)	B (rad)	B <sub>i</sub> (°)	B <sub>i</sub> (rad)	$B_r^2 = B^2 - B_i^2$	B <sub>r</sub> cosθ	sinθ	<D>	Strain
AG70	-22	52.737	26.3685	0.46	0.896052	0.105	0.0018	0.1	0.0017	0.0006	0.0005	0.443948	0.0092	-0.0195
	0 -1 1	37.974	18.987	0.331	0.945718	0.198	0.0035	0.1	0.0017	0.0030	0.0028	0.324989	1.46E-08	-0.9753

Sample No	hkl	2θ(Obs.Max)	θ	θ(rad)	cosθ	B(°)	B (rad)	B <sub>i</sub> (°)	B <sub>i</sub> (rad)	$B_r^2 = B^2 - B_i^2$	B <sub>r</sub> cosθ	sinθ	<D>	Strain
AG80	-22	52.719	26.3595	0.46	0.896052	0.101	0.0018	0.1	0.0017	0.0002	0.0002	0.443948	0.0093	-0.0206
	0 -1 1	37.973	18.9865	0.331	0.945718	0.19	0.0033	0.1	0.0017	0.0028	0.0027	0.324989	1.43E-08	-1.0277

Sample No	hkl	2θ(Obs.Max)	θ	θ(rad)	cosθ	B(°)	B (rad)	B <sub>i</sub> (°)	B <sub>i</sub> (rad)	$B_r^2 = B^2 - B_i^2$	B <sub>r</sub> cosθ	sinθ	<D>	Strain
A100	-22	52.538	26.269	0.458	0.896939	0.125	0.0022	0.1	0.0017	0.0013	0.0012	0.442155	0.0050	-0.0086
	0 -1 1	37.769	18.8845	0.33	0.946042	0.166	0.0029	0.1	0.0017	0.0023	0.0022	0.324043	2.7E-08	-0.4292

## APPENDIX B

### B.1 Image of MO absorption test



Figure B.1: The test of MO absorption

### B.2 Record of MO absorption

Table B.2: The absorbance values of MO in 4 h

Hour	AG50	AG60	AG70	AG80	A100
1	0.604A	0.377A	1.377A	0.395A	0.666A
2	0.600A	0.376A	1.377A	0.391A	0.447A
3	0.597A	0.375A	1.375A	0.390A	0.445A
4	0.598A	0.375A	1.380A	0.391A	0.448A

### B.3 Record of %MO absorption

Table B.3: The %absorption of MO in 4 h

Hour	AG50	AG60	AG70	AG80	A100
1	68.211%	80.158%	27.526%	79.211%	64.947%
2	68.421%	80.211%	27.526%	79.421%	76.474%
3	68.579%	80.263%	27.632%	79.474%	76.579%
4	68.526%	80.263%	27.368%	79.421%	76.421%